

# Review on microstructure and strength-enhancing characteristics of superalloy GH4350

Jin Jufeng<sup>1,2</sup>, Zhao Xinbao<sup>1,3</sup>, Zhao Qianmin<sup>1,2</sup>, Yue Quanzhao<sup>1</sup>, Gu Yuefeng<sup>1,3</sup>, Zhang Ze<sup>1,3</sup>

<sup>1</sup> Institute of Superalloys Science and Technology, School of Materials Science and Engineering, Zhejiang University, Hangzhou 310027, Zhejiang, China; <sup>2</sup> Polytechnic Institute, Zhejiang University, Hangzhou 310027, Zhejiang, China; <sup>3</sup> State Key Laboratory of Silicon and Advanced Semiconductor Materials, Zhejiang University, Hangzhou 310027, Zhejiang, China

**Abstract:** GH4350, or AEREX 350, is a Ni-based wrought superalloy developed for high-performance fasteners operating up to 750°C. It is valued for its high tensile strength, fatigue resistance, stress rupture and relaxation resistance, corrosion resistance, low thermal expansion, and notch sensitivity. GH4350's strength is largely derived from the incorporation of solid solution strengthening elements and the precipitation of  $\gamma'$  phases, along with a minor presence of  $\eta$  phases. However, the alloy's microstructure is sensitive to heat treatment, as  $\gamma'$  phases can transform into  $\eta$  phases under certain conditions, potentially reducing its performance. This transformation is influenced by specific heat treatment parameters, including temperature and time. This review provides an overview of GH4350's chemical composition characteristics, heat treatment strategies and strength-enhancing characteristics, aiming to deepen understanding of the factors behind its remarkable high temperature properties and to guide the development of new alloys or enhancements to boost its temperature capabilities.

**Key words:** fastener wrought superalloy GH4350; high temperature strength; chemical composition; heat treatment;  $\eta$  phase

High-temperature alloy materials are extensively utilized in sectors such as aerospace, energy, and metallurgy due to their capacity to retain superior mechanical properties and structural stability under extreme thermal conditions, where conventional materials would fail due to oxidation, creep, and fatigue<sup>[1-4]</sup>. Typical high-temperature alloy materials include Ni-based superalloys, Co-based superalloys, Al- and Cr-based high-temperature alloys and Pt-Al high-temperature alloys<sup>[2,5-9]</sup>. The demands of the modern aerospace industry, particularly for aero engines, require enhanced thrust-to-weight ratios and greater fuel efficiency at elevated temperatures, thereby necessitating the development of increasingly advanced high-temperature alloy materials<sup>[1,2]</sup>.

Ni-based wrought superalloys are a class of advanced high-temperature alloy materials that exhibit remarkable high temperature properties including resistance to oxidation, fa-

tigue, and creep, and are extensively utilized in diverse industrial sectors, including aerospace, energy, and marine shipping<sup>[5-8]</sup>. Fasteners, which are used extensively in the aerospace industry, represent a crucial category of Ni-based wrought superalloys. Their primary function is to join multiple separate components into a single unit, making fasteners an indispensable element in modern industry<sup>[10]</sup>.

GH4350 stands out as a high temperature Ni-based wrought superalloy used in fasteners due to its ability to withstand service temperatures of up to 750 °C<sup>[11-13]</sup>. Consequently, it must exhibit high tensile and yield strength, along with strong resistance to fatigue, stress rupture, and stress relaxation<sup>[14-17]</sup>. Additionally, corrosion resistance, low thermal expansion and notch sensitivity are critical factors in fastener applications, particularly at elevated temperatures<sup>[15,18]</sup>. The production of high-quality superalloy ingots is crucial for achieving the re-

Foundation item: This work was supported by the Hundred Talents Program of Zhejiang University

Corresponding author: Zhao Xinbao, Ph.D., Professor, Institute of Superalloys Science and Technology, School of Materials Science and Engineering, Zhejiang University, Hangzhou 310027, P. R. China, Tel: +86-0571-64219632, E-mail: [superalloys@zju.edu.cn](mailto:superalloys@zju.edu.cn);

Gu Yuefeng, Ph.D., Professor, Institute of Superalloys Science and Technology, School of Materials Science and Engineering, Zhejiang University, Hangzhou 310027, P. R. China, Tel: +86-0571-64219632, E-mail: [guyf@zju.edu.cn](mailto:guyf@zju.edu.cn);

Copyright © 2019, Northwest Institute for Nonferrous Metal Research. Published by Science Press. All rights reserved.

markable properties required for such demanding applications. Single-melting techniques such as vacuum induction melting (VIM), vacuum arc remelting (VAR) and electro slag remelting (ESR) are utilized to produce high-quality superalloy ingots with fewer oxides, such as  $\text{Al}_2\text{O}_3$  particles<sup>[2,8]</sup>. To further enhance ingot quality, particularly by reducing inclusions, the duplex-melting processes (e.g., VIM+VAR, VIM+ESR) or triple-melting (VIM+VAR+ESR) processes are employed in the melting of GH4350 master ingots<sup>[8,12,19]</sup>.

Following alloy smelting, the microstructure is refined through a combination of cold and hot working techniques along with heat treatment, which are designed based on the chemical composition and microstructure characteristics, to further improve the properties of the alloy<sup>[19]</sup>. Previous research has confirmed that in GH4350, the addition of Co, W and Mo contributes to solid solution strengthening in the face-centered cubic (FCC)  $\gamma$  phase while the addition of Al, Ti, Nb and Ta forms  $\gamma'$  phase which is distributed throughout the  $\gamma$  phase matrix for precipitation strengthening<sup>[12,13,18,20,21]</sup>. In addition to the  $\gamma'$  phase, the formation of the hexagonal close-packed (HCP)  $\eta$  phase is notable. This phase develops during heat treatments and is sensitive to temperature and time<sup>[21,22]</sup>. Understanding the morphology and distribution of  $\eta$  phase is pivotal, as these factors can determine whether its presence is beneficial or detrimental to the alloy's properties<sup>[23–27]</sup>.

This review takes a detailed examination of the chemical composition of GH4350 and various heat treatments, characterized by different microstructures, such as the distribution of  $\gamma'$  and  $\eta$  phases. It aims to offer valuable insights for optimizing chemical composition and enhancing the existing properties of GH4350 with the goal of further increasing its service temperatures.

## 1 Chemical compositions and phase constitutions

### 1.1 The chemical compositions of alloy GH4350

The microstructures of several commonly used Ni-based wrought superalloys for fasteners are summarized in Fig. 1. GH4350, with a service temperature of 750 °C, is derived from the Co-based superalloys MP35N and MP159<sup>[12,28]</sup>. As illustrated in Fig. 1(a), the  $\gamma'$  phases are spherical, with an average diameter of 38 nm, and are uniformly distributed throughout the  $\gamma$  matrix<sup>[15]</sup>. Additionally, plate-like or needle-like  $\eta$  phases predominantly precipitate at grain boundaries, with a smaller fraction of finer  $\eta$  phases forming within the grains<sup>[14,15]</sup>. In contrast, Alloy 718, as depicted in Fig. 1(b) and (c), is primarily strengthened by  $\gamma''$  phases, with a minor presence of spherical  $\gamma'$  phases<sup>[14]</sup>. Also, short rod-like  $\delta$  phases and a small amount of blocky MC carbides are presented on grain boundaries<sup>[14]</sup>. Alloy 718 Plus, shown in Fig. 1(d), is mainly strengthened by  $\gamma'$  phases, accompanied by minor precipitations of  $\eta$  or  $\delta$  phases<sup>[29]</sup>. Furthermore, as illustrated in Fig. 1(e), Waspaloy alloy exhibits a bimodal distribution of  $\gamma'$

phases, comprising spherical primary  $\gamma'$  phases and secondary  $\gamma'$  phases within the matrix, with carbides forming along grain boundaries as a result of heat treatments<sup>[14]</sup>. A similar distribution of  $\gamma'$  phases is observed in GH4698, as shown in Fig. 1(f)<sup>[30]</sup>.

These microstructure differences stem from differences in chemical composition as listed in Table 1. GH4350 contains solid solution strengthening elements like W and Mo, as well as precipitation strengthening elements Al and Ti, leading to the precipitations of  $\gamma'$  phase and  $\eta$  phase. Furthermore, GH4350 adds Ta to improve its mechanical properties. Some reports that the volume fraction of the  $\gamma'$  phase of the alloy samples aged at 850 °C for 4 h is approximately 18 %<sup>[13]</sup>. Obviously, GH4350 differs from other wrought Ni-based superalloys in elemental compositions. Alloy 718 adds more Nb and less (Al+Ti), which leads to precipitations of more  $\gamma''$  phases and less  $\gamma'$  phases<sup>[31–34]</sup>. The volume fraction of  $\gamma''$  phase in a wrought alloy 718 is reported nearly 3 times higher than that of the  $\gamma'$  phase, estimated at 17.8 % and 6.5 %, respectively. However, at temperatures above 650 °C, the  $\gamma''$  phase transforms into the less desirable  $\delta$  phase, which negatively impacts alloy performance. Alloy 718 Plus addresses this issue by increasing Al and Ti content and adjusting the Al/Ti ratio<sup>[35]</sup>. This modification promotes  $\gamma'$  phase precipitation, along with a small amount of  $\eta$  or  $\delta$  phase and raises the service temperature by 55°C<sup>[6,29,36,37]</sup>. Similar to GH4350, optimized additions of Co and W aim to enhance mechanical properties, thermal stability, and stress rupture properties through solid solution strengthening<sup>[29,35]</sup>.

Increasing the volume fraction of the  $\gamma'$  phase in superalloys like alloy 718Plus can enhance their service temperature, however, good processing characteristics are also crucial in wrought superalloys alongside high temperature performance. As shown in Table 1, Waspaloy, lacking Nb, contains three times more Ti than alloy 718Plus, totaling about 5 wt% (Al+Ti), resulting in a  $\gamma'$  phase volume fraction of around 30 % and enables it to withstand temperatures up to 750 °C, higher than alloy 718Plus<sup>[38–41]</sup>. But its processing properties are less favorable compared to alloy 718Plus due to the higher volume fraction of  $\gamma'$  phase and faster  $\gamma'$  phase precipitation<sup>[35]</sup>. A similar issue is likely present in GH4698 which has about 4.5 wt% (Al+Ti) content despite its significant  $\gamma'$  phase volume fraction that improves service temperature, it may also face challenges in processing characteristics. The relatively lower (Al+Ti) content in GH4350 compared to other alloys listed in Table 1 may be intended to moderate  $\gamma'$  phase formation, preventing an excessive increase in deformation resistance, and thus allowing GH4350 to maintain a favorable combination of strength and deformability.

#### 1.1.1 Solid solution strengthening elements

The Ni-based  $\gamma$  phase of the matrix characterized by a FCC crystal structure can dissolve some alloying elements primarily including Co, Cr, Mo, and W. These solute elements inter-

act with matrix and cause lattice misfit and modulus misfit which will impede dislocation movement and enhance the performance of superalloys<sup>[42,43]</sup>.

The solid solution strengthening effect of each element  $i$  ( $\Delta\sigma_{SSi}$ ) has been quantitatively evaluated in Ni- $X_i$  binary alloy systems by many researchers and they believe that the solid solution strengthening effect results from the interaction of solute atoms with dislocations<sup>[43-50]</sup>. On this basis,  $\Delta\sigma_{SSi}$  can be calculated by<sup>[51,52]</sup>:

$$\Delta\sigma_{SSi} = K_i c_i^{1/2} \quad (1)$$

where  $K_i$  and  $c_i$  are strengthening constant and atomic percentage of solute element  $i$ , respectively.

In the case of multi-component Ni-based superalloys, the total solid solution strengthening effects ( $\Delta\sigma_{SS}$ ) can be assessed by the method of Gypen and Deruyttere<sup>[53]</sup>:

$$\Delta\sigma_{SS} = (\sum_i \Delta\sigma_{SSi}^2)^{1/2} \quad (2)$$

Combining Eq. (1) and Eq. (2), the  $\Delta\sigma_{SS}$  is expressed as:

$$\Delta\sigma_{SS} = (\sum_i K_i^2 c_i)^{1/2} \quad (3)$$

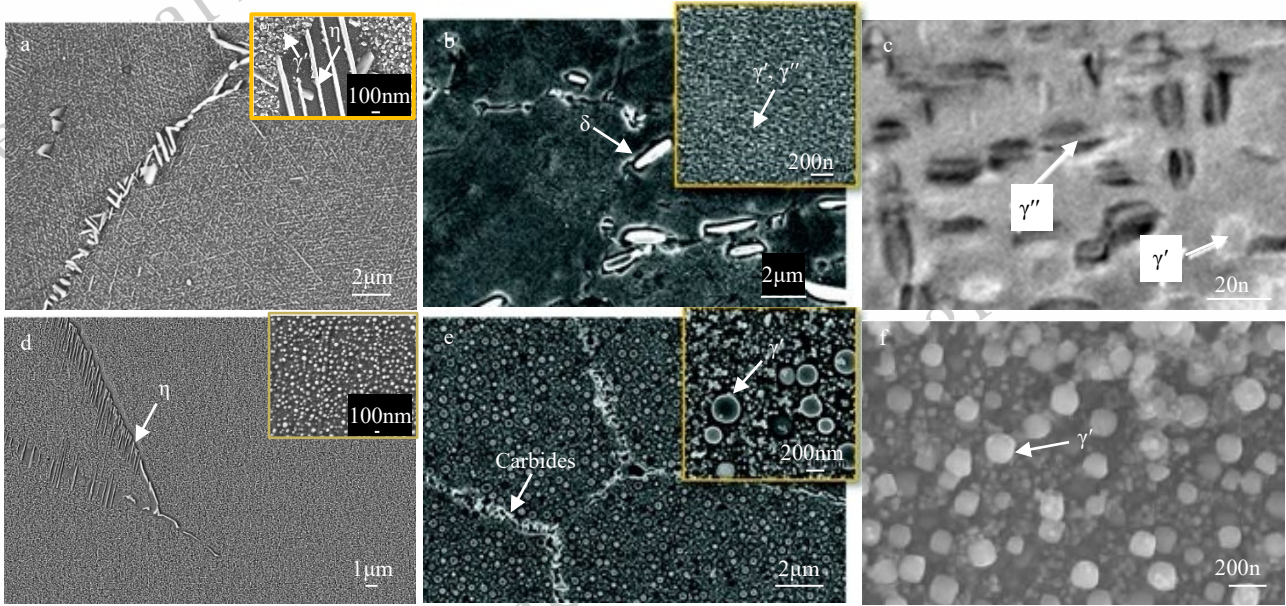


Fig. 1 Typical microstructures of Ni-based wrought superalloys. (a) Microstructure of GH4350. (b) and (c) Microstructure of alloy 718. (d) Microstructure of alloy 718Plus. (e) Microstructure of Waspaloy alloy. (f) Microstructure of GH4698. (adapted from Refs.<sup>[14,15,29,30,54]</sup>)

**Table 1 Chemical compositions of typical Ni-based wrought superalloys for fasteners(wt%)**<sup>[22,35,41,55]</sup>

Ni-based	Ni	Cr	Co	Mo	W	Nb	Al	Ti	Fe	C	P+B	Ta
718	Bal.	19	/	3.0	/	5.15	0.6	0.9	18.5	0.04	0.01	/
718 Plus	Bal.	18.0	9.1	2.7	1.0	5.4	1.45	0.75	9.5	0.020	0.011	/
Waspaloy	Bal.	19.0	13.5	4.0	/	/	1.9	3.0	/	0.07	0.005	/
GH4698	Bal.	14.68	/	3.05	/	2.09	1.68	2.7	0.47	0.048	/	/
GH4350	Bal.	17	25	3	2	1.2	1.0	2.2	/	≤0.025	≤0.025	4

$K_i$  can be determined by analyzing 0.2 % flow stress experimental data on the solution strengthening of Ni- $X_i$  binary alloys<sup>[51,52]</sup>. The results are shown in Fig. 2. Elements with larger  $K_i$  generally indicate a greater potential for solid solution strengthening such as Mo, W, Ta and Nb. It is reasonable for major precipitation strengthening element Al to obtain a low strengthening constant.

The addition of a large amount of Co is one distinguishing feature of GH4350 compared to other Ni-based wrought superalloys. As shown in Fig. 2, adding Co atoms contribute to solid solution strengthening. In addition, as a matrix element, Co facilitates the transformation of part of the  $\gamma$  matrix from

FCC to HCP which induces a strengthening effect by the presence of two distinct crystal structures creating a barrier to dislocation motion during cold working<sup>[18,56,57]</sup>. Another important impact of Co addition is its influence on stacking defects. Co reduces stacking fault energy which inhibits the cross-slip motion of dislocations, thereby suppressing dislocation annihilation and improving the ability of twinning, leading to enhanced strain hardening capability of the superalloys<sup>[58]</sup>.

In addition, firstly, solid solution strengthening elements are effective only if they successfully enter the matrix. Therefore, these elements must preferentially partition to the  $\gamma$  matrix.



Alloying elements can be categorized into two groups based on their partitioning coefficient  $k_i^{\gamma'}$ , as defined below<sup>[59]</sup>:

$$k_i^{\gamma'} = \frac{c_i^{\gamma'}}{c_i^{\gamma}} \quad (4)$$

where  $c_i^{\gamma'}$  and  $c_i^{\gamma}$  represent the atomic fractions of element  $i$  in the  $\gamma'$  and  $\gamma$  phases, respectively. Elements such as Co, Cr, Mo, and W are typically enriched in the  $\gamma$  phase (with  $k < 1$ ), whereas elements like Al, Ti, and Ta tend to be enriched in the  $\gamma'$  phase. (with  $k > 1$ )<sup>[59,60]</sup>.

Secondly, these solid solution strengthening elements must form a stable solid solution in the  $\gamma$  matrix, which can continuously hinder dislocation movement. To maintain their strengthening effect, especially at high temperatures, these elements should not diffuse extensively. This requires a low diffusion rate in the matrix. The diffusion coefficient of element  $i$  in the  $\gamma$  phase at temperature  $T$ , denoted as  $D_T^{i, Ni}$ , is given as follows<sup>[61–64]</sup>:

$$D_T^{i, Ni} = D_0^{i, Ni} \exp\left(\frac{-Q^{i, Ni}}{RT}\right) \quad (5)$$

where  $D_0^{i, Ni}$  and  $Q^{i, Ni}$  are the pre-exponential factor and the activation energy for interdiffusion of element  $i$  in Ni, respectively.

For example, when calculating the diffusion coefficients of the elements at 800°C, the results in Table 2 demonstrate that the diffusion coefficients vary significantly among the elements. Specifically, the diffusion coefficients of Nb, Ta, Ti, and Al are higher, while those of Cr, Co, Mo, and W are lower. As a result, the latter elements diffuse more slowly at high temperatures, thereby better maintaining the solid solution strengthening effect.

Table 2 diffusion coefficient calculation of typical elements at  $T = 800^\circ\text{C}$ <sup>[61,62,65,66]</sup>

element	$D_0^{i, Ni}$ ( $\text{m}^2/\text{s}$ )	$Q^{i, Ni}$ (kJ/mol)	$D_T^{i, Ni}$ ( $\text{m}^2/\text{s}$ ) $T=800^\circ\text{C}$
Cr	$5.2 \times 10^{-4}$	289	$4.45 \times 10^{-18}$
Co	$1.8 \times 10^{-4}$	282	$3.38 \times 10^{-18}$
Mo	$1.15 \times 10^{-4}$	281	$2.41 \times 10^{-18}$
W	$8.6 \times 10^{-6}$	264	$1.21 \times 10^{-18}$
Nb	$8.8 \times 10^{-5}$	257	$2.72 \times 10^{-17}$
Ta	$2 \times 10^{-5}$	251	$1.21 \times 10^{-17}$
Ti	$4.1 \times 10^{-4}$	275	$1.69 \times 10^{-17}$
Al	$4.3 \times 10^{-4}$	272	$2.48 \times 10^{-17}$

In addition to the incorporation of Co, the GH4350 alloy also contains W and Mo, with a combined total mass fraction of 5%. Both W and Mo exhibit relatively high solid solution strengthening constants, indicating their significant contribution to the solid solution strengthening of the alloy<sup>[67]</sup>. These elements primarily partition to the  $\gamma$  matrix phase, and their diffusion coefficients at high temperatures are relatively low, which minimizes their tendency to diffuse out of the matrix. As a result, they effectively maintain the solid solution

strengthening effect, thereby significantly enhancing the alloy's strength at elevated temperatures.

### 1.1.2 Precipitation strengthening elements

Al, Ti and Nb are typical  $\gamma'$  phase formers and  $\gamma'$  phase remains stable at high temperatures, effectively hindering dislocation motion. An increase in Al, Ti and Nb content increases the  $\gamma'$  phase volume fraction, which further enhance the alloy's strength. GH4350 contains a combined weight percentage of 4.5 % of Al, Ti and Nb which signifies a significant potential for precipitation strengthening within the alloy.

In addition to Al, Ti and Nb, Ta also plays a vital role in strengthening the  $\gamma'$  phase and represents a notable difference in the composition of GH4350 compared to other Ni-based wrought superalloys. Ta is not commonly found in Ni-based wrought superalloys but is frequently used in Ni-based single crystal superalloys. This discrepancy arises because excessive  $\gamma'$ -phase-forming elements can increase the deformation resistance in Ni-based wrought superalloys, thereby diminishing their cold or hot workability<sup>[68]</sup>. Conversely, Ni-based single crystal superalloys are cast directly without undergoing cold or hot working processes, allowing for the inclusion of higher amounts of  $\gamma'$ -phase-forming elements.

The Ta content can varies from 3 wt% to 12 wt% and the total amount of main  $\gamma'$ - phase-forming elements(Al+Ti+Ta) could exceed up to 20 wt%<sup>[69,70]</sup>. As a result, the volume fraction of  $\gamma'$  phase of Ni-based single crystal superalloys can surpass 60 wt%<sup>[71–74]</sup>. Researchers have shown that Ta inhibits the coalescence of the  $\gamma'$  phase during isothermal long-term aging, thereby improving the microstructure stability of the  $\gamma'$  phase and increasing its volume fraction<sup>[74–78]</sup>. Additionally, Ta can enhance oxidation and thermal corrosion resistance of superalloys in certain conditions<sup>[79,80]</sup>.

The addition of Al, Ti, Nb and Ta of GH4350 actively contributes to maintaining the structural integrity and stability of the  $\gamma'$  phase, effectively inhibiting its dissolution or structural alterations at elevated temperatures. Consequently, the  $\gamma'$  phase continues to impede dislocation motion at high temperatures, thereby strengthening the alloy. This enhancement in  $\gamma'$  phase stability is pivotal for ensuring the alloy retains its desired properties.

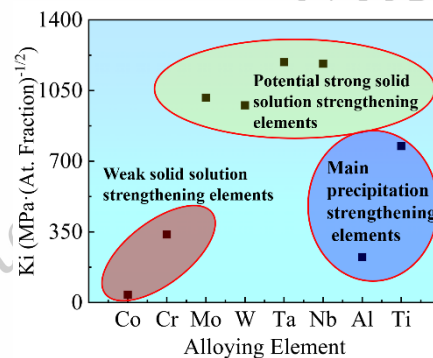


Fig. 2 Strengthening constants for solid solution strengthening in Ni.

(adapted from Ref. [51])

## 1.2 The precipitation phases of GH4350

Many studies have demonstrated that the precipitation phases of GH4350 are  $\gamma'$  phase and  $\eta$  phase [12–15,20–22,28,56,68,81,82]. The crystal structure of  $\eta$  phase is shown in Fig. 3(a). Apparently, the stacking sequence is ABACABAC....., which is a typical kind of HCP crystal structure. Fig. 3(b) and (c) indicates the microstructure of  $\gamma'$  phase and  $\eta$  phase by transmission electron microscope (TEM) and the chemical compositions of them of alloy K4750 respectively. The energy dispersive spectrometer (EDS) results show that the  $\eta$  phase are primarily composed of Ni, Al, Ti, Nb, which are close to the chemical composition of  $\gamma'$  phase.

## 1.3 Heat treatment of GH4350

### 1.3.1 Homogenization of as-cast GH4350

Due to their high degree of alloying, wrought superalloys often experience severe dendritic segregation during solidification, leading to poor hot workability [83]. To eliminate the segregation, an appropriate homogenization heat treatment process is essential and is the first step to obtain the target microstructure [83–85]. In the as-cast state of GH4350 prepared by VIM+VAR, significant elemental segregation occurs with Nb, Ti and Ta elements enriched in the in-

ter-dendrites, and Cr, Mo and Al elements enriched in the dendrites [11]. This segregation is accompanied by the precipitation of Laves phases and acicular phases in the inter-dendrites, while dispersed  $\gamma'$  phases are also precipitated during the cooling process [11]. To mitigate these issues, a homogenization heat treatment at 1180 °C for 40 h with furnace cooling has been proposed, successfully eliminating elemental segregation and detrimental phases [11]. Achieving a uniform microstructure with consistent elemental composition requires a relatively long heat treatment time, and researches on homogenization heat treatments are limited. Therefore, careful design of the melting and homogenization processes is crucial.

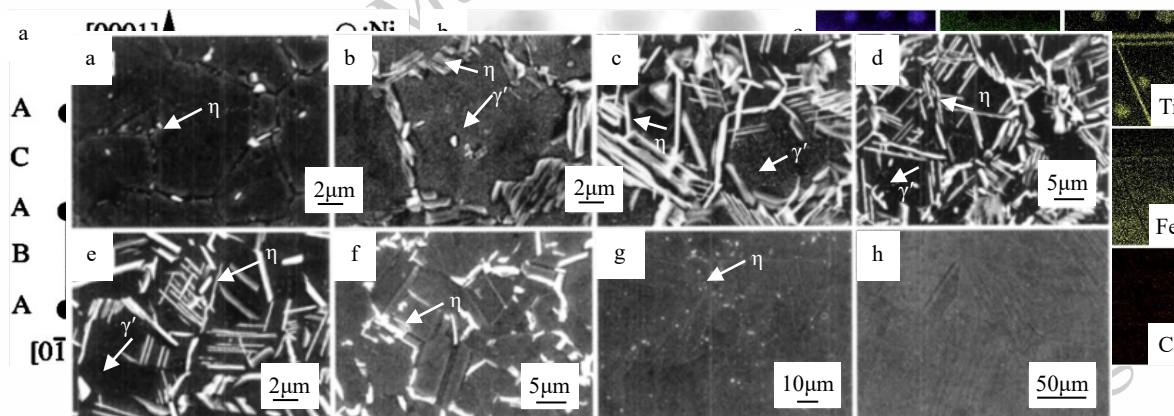
### 1.3.2 Solid solution heat treatment of GH4350

Precipitation phases can be detrimental if they form excessively during solidification, as they can act as sources of cracks. However, these phases are also crucial for precipitation strengthening. Therefore, a comprehensive understanding of the control of precipitation phases in GH4350 is essential. Scanning electron microscope (SEM) observations of samples solution-treated at various temperatures for 1 h

Fig. 3 Crystal structure and chemical composition of  $\eta$  phase. (a) Crystal structure of  $\eta$  phase. (b) The TEM image of  $\gamma'$  and  $\eta$  phase and (c) the corresponding EDS mapping of alloy K4750. (adapted from Refs. [86,87])

are shown in Fig. 4. The  $\gamma'$  phases begin to dissolve at 1010 °C which aligns well with the solvus temperature of  $\gamma'$  phases reported in other literatures [12,81].

at 1055 °C. When the temperature rises to 1080 °C, only sporadic  $\eta$  phase can be observed and it is completely dissolved at 1095 °C.



As indicated in Fig. 4, the  $\eta$  phase is significantly reduced

Fig. 4 SEM observations of samples solution-treated at different temperatures for 1 h. (a)–(h) are solution-treated at 830 °C, 950 °C, 980 °C, 1010 °C, 1020 °C, 1055 °C, 1080 °C and 1095 °C respectively. (adapted from Ref. [82])

If the alloy is solid-solution treated below the solvus temperature of the  $\eta$  phase, such as at 1050 °C, the precipitation of the  $\eta$  phase at grain boundaries may be utilized to control grain size like  $\delta$  phase [20,88]. As the temperature increases from 800 °C to 1070 °C, the recrystallized grain size increases

slightly from approximately 10 μm to 14 μm while further increasing temperature from 1080 °C to 1095 °C, the grain size increases significantly, approaching 100 μm, due to the lack of  $\eta$  phase pinning at the grain boundaries [82]. Most reported solid-solution temperatures of GH4350 are above the solvus

temperature of the  $\eta$  phase<sup>[12,13,15,21,68,89]</sup>. It appears that controlling grain size with the  $\eta$  phase is not the primary focus of the solid-solution treatment but the complete dissolution of  $\eta$  phase into the matrix is the ultimate goal. This approach may help to prevent the continued growth of the  $\eta$  phase during solid solution heat treatment<sup>[22]</sup>.

### 1.3.3 Aging treatment of GH4350

Aging treatments are performed after solid solution to optimize the precipitations of  $\gamma'$  and  $\eta$  phases<sup>[90]</sup>. The lower limit temperature of  $\gamma'$  phase precipitation is determined to be between

650 °C and 700 °C based on variation in hardness over aging time and temperature (Fig. 5(a)) for solution-treated GH4350 alloy<sup>[12,81]</sup>.

During aging treated at 788 °C, the  $\eta$  phase is observed at the grain boundaries (Fig. 5 (b), point C<sub>1</sub>), indicating that the lower limit for  $\eta$  phase precipitation is approximately 788 °C. When the aging temperature is further increased to 816 °C, maximum hardness is achieved at both solid solution temperatures. As seen at point D<sub>1</sub> in Fig. 5(b), both  $\gamma'$  and  $\eta$  phases are present.

As indicated in Fig. 5(c) through (f), the growth and morphology of the  $\eta$  phase vary with different heat treatments. Initially, the plate-like  $\eta$  phase precipitates at the grain boundaries (Fig. 5(c) and (d)). With increasing aging temperature and time, the  $\eta$  phase progressively grows from the grain boundaries to the grains, forming a Widmanstätten morphology structure (Fig. 5(e) and (f)).

In conclusion, the precipitation and distribution characteristics of the  $\eta$  phase are significantly affected by the aging heat treatment. A comprehensive understanding of the effect of heat treatment on  $\gamma'$  and  $\eta$  phases precipitation is required to develop a rational heat treatment strategy.

### 1.4 Phase transformation behaviors

From the perspective of phase stability, the  $\eta$  phase is a more stable at temperatures of 650 °C or above, which is confirmed by thermodynamic calculations of the phase stability of Nimonic 263 that show the  $\gamma'$  phase is stable up to 750 °C while  $\eta$  phase is stable up to 957 °C<sup>[91]</sup>. Long-term thermal exposure further supports this, as the  $\eta$  phase predominates throughout the matrix, and nearly all  $\gamma'$  particles dissolve when the alloy is exposed to 870 °C for 8000 h<sup>[92]</sup>.

The chemical compositions of the  $\gamma'$  and  $\eta$  phases are similar with their primary distinction being their crystal structures. The  $\gamma'$  to  $\eta$  transformation occurs through the introduction of stacking faults into the  $\gamma'$  phase formed by the systematic passage of Shockley partials<sup>[68,87,91–96]</sup>. As shown in Fig. 6, theoretically, if one A layer is added by the introduction of extrinsic stacking faults in  $\gamma'$  between B layer and C layer, the stacking sequence will become ABACABAC ... which is actually identical to the stacking sequence along the close packed planes (0001) in  $\eta$  phase. Experimental observations, as shown in Fig. 7(a)~(d), indicate that the  $\eta$  phase grows at the expense of  $\gamma'$  phase, with  $\gamma'$  precipitation-free zones (PFZs) forming around each  $\eta$  precipitate. The above information suggests a close relationship between  $\eta$  phase formation, the  $\gamma'$  phase, and stacking

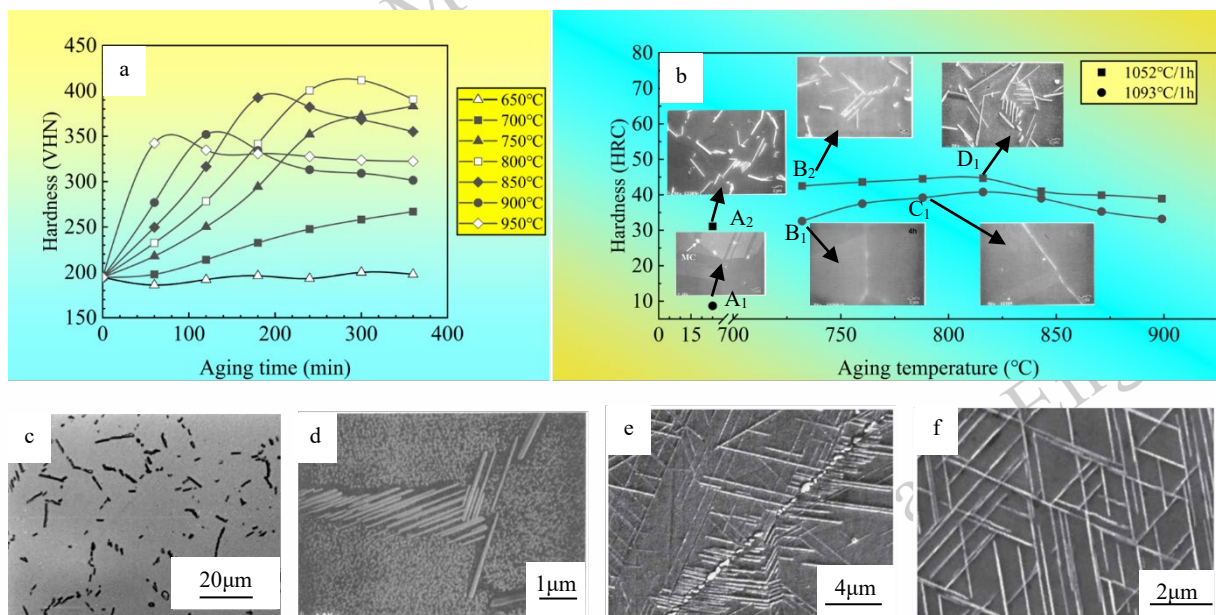


Fig. 5 Microstructures corresponding to different heat treatment and their associated hardness values. (a) Variation of hardness with aging time for solution-treated GH4350 at various temperatures. (b) Variation of hardness with aging temperature for solution-treated GH4350 and the corresponding microstructures for several typical points (A to D). (c) and (d) are both solid solution-treated at approximately 1050 °C for 1h but aging-treated at 750 °C for 1h and at 899 °C for 4h+816 °C for 4h respectively. (e) and (f) are solid solution treated at 1100 °C for 1h+ aging-treated at 1000 °C for 3h and (e) is grain boundary area while (f) is grain interior. (adapted from Refs. <sup>[12,22,81]</sup>)



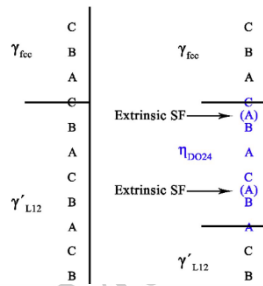


Fig. 6 Illustration of the  $\gamma'$  to  $\eta$  transformation by the introduction of extrinsic stacking faults. (adapted from Refs. [86,87])

faults. Additionally, Fig. 7(e)~(h) demonstrates that stacking faults, induced by numerous paired dislocations, appear to elongate and eventually transform into the growing  $\eta$  phase at the expense of  $\gamma'$  phase.

More precise evidence in experiment indicates that two-layer extrinsic faults found in  $\gamma'$  phase (Fig. 8(a) and (b)) are formed by the passage of two identical  $1/6\langle 112 \rangle$  shockley partials on consecutive  $\{111\}$  planes and  $\eta$  phase forming elements (i.e., Ta, Nb, Ti) are segregated along superlattice extrinsic stacking faults (SESFs) confirmed by high spatial resolution energy dispersive X-ray spectroscopy (EDX) mapping (Fig. 8(c)) [93,94].

These observations indicate that stacking faults in the  $\gamma'$  phase may serve as local nucleation sites for the  $\eta$  phase. Fig. 9(a) and (b) shows that the nucleation and growth of  $\eta$  phase have two paths which  $\eta$  phase directly precipitates within extra-large  $\gamma'$  (EL- $\gamma'$ ) when the coalescence of  $\gamma'$  phases reaches a critical stage or  $\eta$  phase precipitates at the interface between

small MC carbides and EL- $\gamma'$  with both MC carbides and  $\eta$  embedded within EL- $\gamma'$  [40].

Interestingly, as shown in Fig. 9(c) and (d), both paths share a common feature: they both lead to the formation of stacking faults. Notably, MC carbides are segregated with Ti and the nucleation and growth of  $\eta$  phase in the second path (with MC-II carbide) occur more rapidly than in the first path (without carbide) [40]. This suggests that MC-II carbide is a more effective provider of  $\eta$  phase-forming elements compared to EL- $\gamma'$  in this study.

Based on the preceding discussion, two criteria for the formation and growth of the  $\eta$  phase can be concluded: (1) stacking faults initially serve as nucleation sites, and (2) sufficient  $\eta$  phase-forming elements must be present during nucleation and growth. To better regulate the microstructure and, consequently, the properties of superalloys, further research into the mechanisms of  $\eta$  phase nucleation and growth is necessary. This will enhance our understanding and control over  $\eta$  phase development.

## 2 Roles of $\eta$ phase

To address the need for higher operating temperatures in fasteners, increasing the amount of  $\gamma'$  phase strengthening elements may enhance high-temperature performance. However, at temperatures above 650 °C, the  $\gamma'$  to  $\eta$  phase transformation occurs, leading to a decrease in the  $\gamma'$  phase volume fraction and consequently reducing its reinforcing effect. Therefore, understanding the impact of the  $\eta$  phase on the properties of superalloys is crucial.

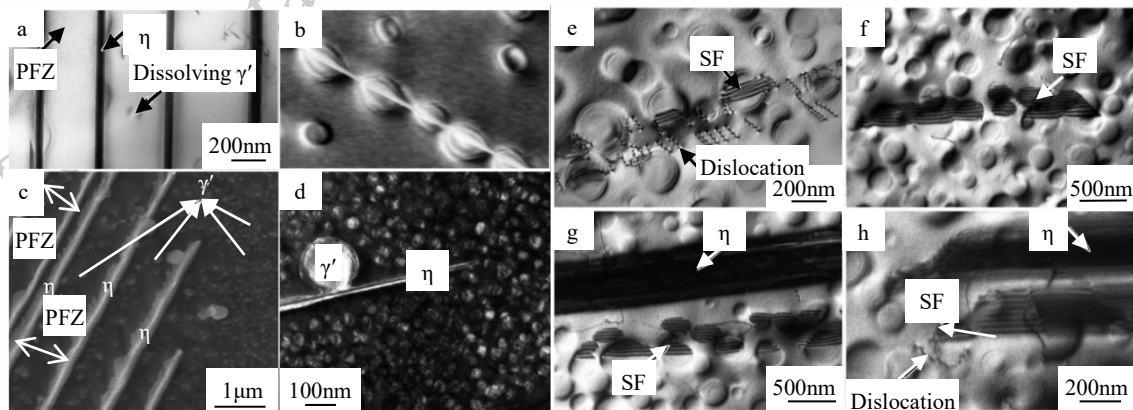


Fig. 7 Typical micrographs of  $\eta$  phase growing by consuming  $\gamma'$  phase of various superalloys. (a) Alloy K4750. (b) Alloy GH4350. (c) Alloy A286. (d) Alloy 718 plus. (e)~(h) are TEM images of stacking faults and  $\eta$  phase in K4750. (adapted from Refs. [68,87,95,96])

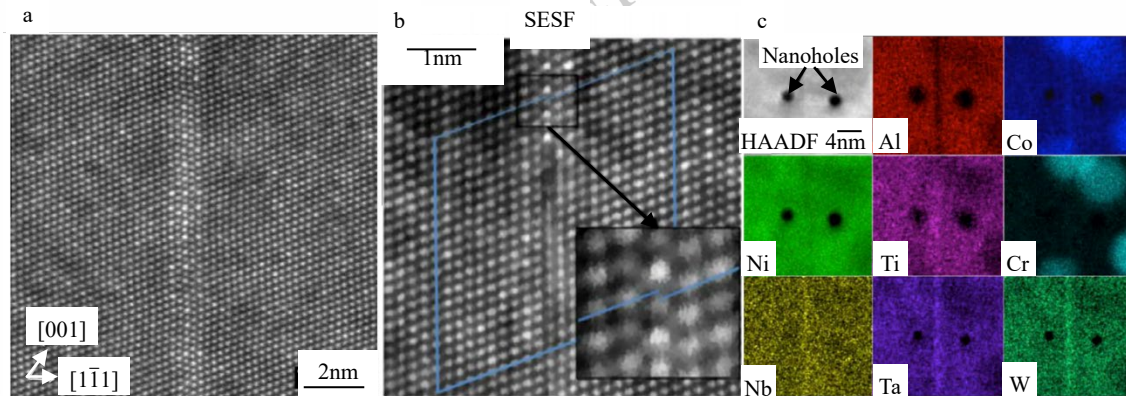


Fig. 8 More precise evidence of  $\gamma'$  phase to  $\eta$  phase transformation in experiment. (a) High angle angular dark field-scanning transmission electron microscope (HAADF-STEM) images of a grid-like ordering along a SESF inside a  $\gamma'$  precipitate; (b) Shockley partials at leading SESF showing by burgers circuit analysis. (c) EDX elemental map of a vertical SESF showing segregation along the fault. (adapted from Ref. [93])

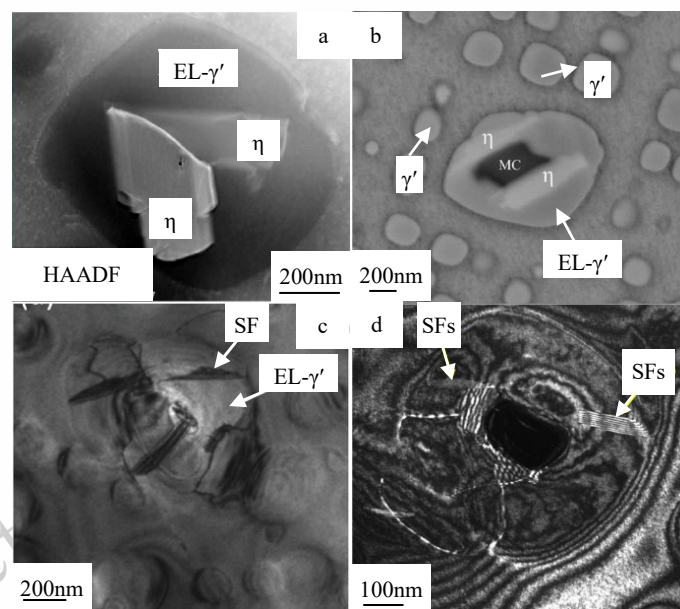


Fig. 9 Two paths of  $\eta$  phase formation. (a) Precipitate directly within EL- $\gamma'$ . (b) Precipitate at the interface of small size MC carbides and EL- $\gamma'$ . (c) and (d) are the formation of stacking faults in both paths, respectively. (adapted from Ref. [40])

As previously discussed, the  $\eta$  phase initially precipitates at the grain boundaries (intergranular) and evolves into a Widmanstätten morphology with increased time and temperature (intragranular). Researchers have identified four distinct forms of the  $\eta$  phase—needle-like, plate-like, granular, and short rod-like (Fig. 10), each of which impacts the properties of superalloys differently<sup>[23,95]</sup>.

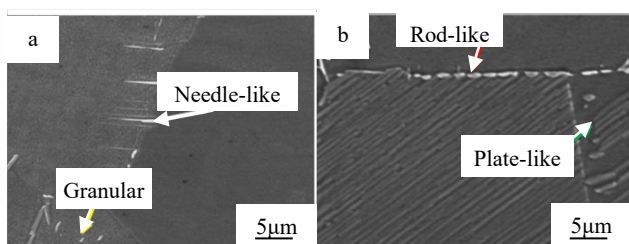


Fig. 10 Needle-like, plate-like, granular and short rod-like  $\eta$  phase. (adapted from Ref. [23])

This characteristic affects the morphology of grain boundaries, significantly impacting superalloy strengthening. It is reported that the discontinuous precipitation of plate-like  $\eta$  phase exerts a pinning effect on the grain boundary, leading to the formation of grain boundary serrations whose magnitude is increased with the increase of the inclination angle with respect to the grain boundaries<sup>[6,29,95]</sup>. Grain boundary serrations, intergranular and intragranular  $\eta$  phase influence the properties of superalloys.

## 2.1 The effects of $\eta$ phase on crack initiation and propagation

Serrated grain boundaries induced by  $\eta$  phase can enhance the creep resistance by reducing cavitation and crack propagation rates and they also appear to retard the propagation of intergranular cracks to some extent



during fatigue test<sup>[25,26]</sup>. This suggests a potential beneficial effect of the  $\eta$  phase-induced serrated grain boundaries in impeding crack propagation along grain boundaries.

Additionally, small  $\eta$  phases at grain boundaries typically do not initiate cavities during creep though dislocations piled up ahead of them<sup>[87]</sup>. As shown in Fig. 11(a), 2 to 3% area fraction of  $\eta$  phase which extended from grain boundaries across the PFZs may be beneficial to creep strength and ductility by constraining grain boundary cavity growth<sup>[24]</sup>. These findings collectively indicate that the  $\eta$  phases whether in small sizes at grain boundaries or within a limited area fraction may not necessarily have a detrimental effect on creep properties. Instead, in certain configurations, they may exhibit a neutral or even a beneficial role in enhancing creep strength and ductility by impeding cavity growth along grain boundaries.

However, as illustrated in Fig. 11(b) and (c), cracks tend to form around the  $\eta$  phases, indicating intergranular  $\eta$  phase may act as brittle sites at the grain boundaries, thus serving as sites for crack initiation during creep tests<sup>[27]</sup>. During the fatigue processes, stress concentration as a result of dislocations accumulation and networks formation at the edges of  $\eta$  precipitates can induce the initiation and propagation of micro-cracks<sup>[25]</sup>. These observations suggest that the impact of  $\eta$  phases on crack initiation and propagation varies depending on specific conditions, such as loading type (creep or fatigue) and microstructural characteristics, underscoring the complexity and multifaceted nature of the  $\eta$  phase in superalloys.

Understanding the circumstances under which the  $\eta$  phase acts as a crack initiation site or stress concentrator versus when it potentially impedes crack propagation is crucial. This understanding will greatly aid in optimizing superalloy designs to harness beneficial effects or mitigate detrimental influences of the  $\eta$  phase on properties.

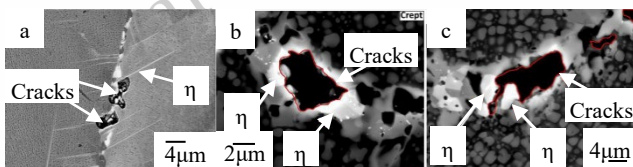


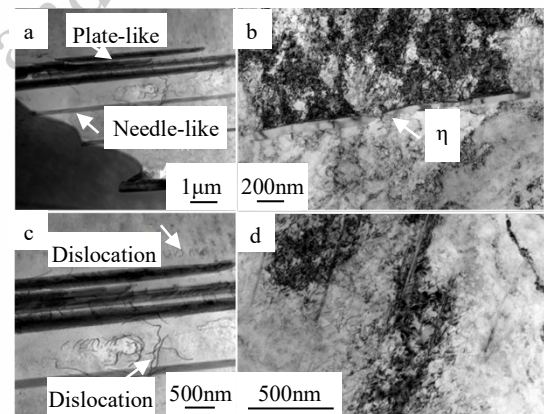
Fig. 11 The role of  $\eta$  phase during creep test. (a) Two grain boundary cavities whose growth appears to be constrained by impingement on  $\eta$  phase platelet. (b) and (c) are backscattered electron micrographs of STAL15-CC alloy after creep at 850 °C showing secondary cracks forming around  $\eta$  layers at grain boundaries. (adapted from Refs. <sup>[24,27]</sup>)

## 2.2 The effects of $\eta$ phase on dislocation hindering

As a precipitation phase,  $\eta$  phase is expected to contribute to precipitation strengthening similar to the  $\gamma'$  phase. For instance, with aging time extending from 25 h to 100 h, the ultimate tensile strength (UTS) of alloy ATI 718Plus signifi-

cantly improves from 797 MPa to 860 MPa with an increased volume fraction of plate-like/needle-like  $\eta$  phases<sup>[23]</sup>. Notably, during this period, the volume fraction of  $\gamma'$  phase decreases from approximately 32 % to 28 %<sup>[23]</sup>. This suggests that the strengthening effect of the  $\gamma'$  phase is comparatively weaker. Consequently, the observed enhancement in tensile properties is attributed to the precipitation of a significant amount of plate-like and needle-like  $\eta$  phases. TEM observations further confirm that the improved UTS is due to the hindrance of dislocation motion at grain boundaries and within grains near the  $\eta$  phases (Fig. 12(a) and (c)).

The effect of  $\eta$  phase on dislocation hindering is also reported in a research of stress relaxation behavior of GH4350, it is concluded that the enhanced stress relaxation resistance at 800 °C is attributed to the dislocation blocking by  $\eta$  phases, as shown in Fig. 12(d)<sup>[15]</sup>. This study also compares the stress relaxation resistance of Waspaloy and GH4350 at various temperatures. At 600 °C, dislocations are still impeded by intragranular  $\eta$  phases (Fig. 12(b)), however, the larger size and higher mass fraction of  $\gamma'$  phases in Waspaloy are key factors in hindering the movement of dislocations while the amount of intragranular  $\eta$  phases in GH4350 is rather small, thus  $\eta$  phases contribute little to the relaxation resistance at this tem-



perature, leading a better stress relaxation resistance of Waspaloy than that of GH4350<sup>[15]</sup>.

Fig. 12 Bright-field TEM observations of  $\eta$  phases and the dislocations. (a) Grain boundary  $\eta$  phases and the dislocations in the grain, (c) is the high magnifications of (a). (b) and (d) are microstructures of GH4350 after relaxation at 600 °C and 800 °C respectively. (adapted from Refs. <sup>[15,23]</sup>)

## 3 Conclusions

1) GH4350 incorporates significant amounts of Co, Mo, and W to enhance solid solution strengthening, as quantified through modeling, and maintains a moderate (Al+Ti+Nb) content to balance precipitation strengthening with deformability. The addition of Ta not only stabilizes and increases the volume fraction of the  $\gamma'$  phase but also improves oxidation and thermal corrosion resistance.

2) The primary precipitation phases in GH4350 are  $\gamma'$  and  $\eta$ ,

which can be controlled through heat treatment at various temperatures and durations. A homogenization heat treatment at 1180 °C for 40 h with furnace cooling effectively removes elemental segregation and undesirable phases, providing a foundation for subsequent phase control.

3) The lower temperature limit for  $\gamma'$  phase precipitation is between 650 °C and 700 °C, with a solvus temperature around 1010 °C. For  $\eta$  phase, precipitation begins at approximately 788 °C. As temperature and time increase,  $\eta$  phase precipitates from grain boundaries into the grains, developing a Widmanstätten morphology, and eventually dissolves completely at temperatures nearing 1080 °C. Solid solution heat treatment below this temperature may be able to control grain size through the undissolved  $\eta$  phase.

4) The  $\gamma'$  to  $\eta$  phase transformation occurs because  $\eta$  phase is more stable above 650 °C. Both phases share similar elemental compositions and transformable crystal structures, facilitated by the introduction of stacking faults. This transformation is accelerated in the presence of effective  $\eta$  phase-forming elements providers, such as MC-type carbides, surrounding the  $\gamma'$  phase.

5) Small quantities of  $\eta$  phase with needle-like, plate-like, granular, and short rod-like morphologies can improve properties such as creep resistance, tensile strength, fatigue resistance, and stress relaxation resistance by reducing cavitation, crack propagation, and hindering dislocation movement. Conversely, a large volume of  $\eta$  phase with Widmanstätten morphology can negatively impact mechanical properties, as the brittleness of  $\eta$  phase and associated stress concentrations lead to crack initiation and growth, ultimately depleting  $\gamma'$  phase and diminishing its strengthening effect.

## References

- PAN Y, WEN M. Ab-initio calculations of mechanical and thermodynamic properties of TM (transition metal: 3d and 4d)-doped Pt3Al[J]. *Vacuum*, 2018, 156: 419-426.
- PAN Y, PU D L, LI Y Q, et al. Origin of the antioxidation mechanism of RuAl(1 1 0) surface from first-principles calculations[J]. *Materials Science and Engineering: B*, 2020, 259: 114580.
- PAN Y, YANG F. Influence of pressure on the structural, elastic and thermodynamic properties of  $\alpha$ - and  $\beta$ - PtAl high temperature alloys[J]. *Journal of Materials Research and Technology*, 2024, 28: 381-389.
- PAN Y. Vacancy-induced mechanical and thermodynamic properties of B2-RuAl[J]. *Vacuum*, 2017, 143: 165-168.
- LIANG L, XU M, CHEN Y, et al. Effect of welding thermal treatment on the microstructure and mechanical properties of nickel-based superalloy fabricated by selective laser melting[J]. *Materials Science and Engineering: A*, 2021, 819: 141507.
- PICKERING E J, MATHUR H, BHOWMIK A, et al. Grain-boundary precipitation in Allvac 718Plus[J]. *Acta Materialia*, 2012, 60(6-7): 2757-2769.
- CHEN T W, WANG P T, KANG Y C, et al. Grain boundary serration tuning and its effect on hot workability of a wrought superalloy[J]. *Journal of Alloys and Compounds*, 2023, 960: 170620.
- FECHT H, FURRER D. Processing of Nickel-Base Superalloys for Turbine Engine Disc Applications[J]. *Advanced Engineering Materials*, 2000, 2(12): 777-787.
- PAN Y. Exploring the phase stability, mechanical and thermodynamic properties of FeCrAl ternary alloy[J]. *Journal of Materials Research and Technology*, 2023, 26: 8813-8821.
- MELHEM G N. Encyclopedia of Aluminum and Its Alloys, Two-Volume Set (Print) [M]. 1st ed. Boca Raton: CRC Press, 2018.
- LI K, YANG Y, WANG Z, et al. Micro-segregation and homogenizing treatment of GH350 ingot[J]. *Journal of Iron and Steel Research International*, 2012, 24(7): 54-58. (in Chinese)
- ASGARI S. Age-hardening behavior and phase identification in solution-treated AEREX 350 superalloy[J]. *Metallurgical and Materials Transactions A*, 2006, 37(7): 2051-2057.
- NAJAFI H, ASGARI S. Strain hardening mechanisms in aged AEREX350 superalloy[J]. *Materials Science and Engineering: A*, 2005, 398(1-2): 204-208.
- JIANG H, YANG J, DONG J, et al. Stress Relaxation Behavior Comparison of Typical Nickel-Base Superalloys for Fasteners[C]// Proceedings of the 9th International Symposium on Superalloy 718 & Derivatives: Energy, Aerospace, and Industrial Applications. Cham: Springer International Publishing, 2018: 789-804.
- WANG Y, DONG J, ZHANG M, et al. Stress relaxation behavior and mechanism of AEREX350 and Waspaloy superalloys[J]. *Materials Science and Engineering: A*, 2016, 678: 10-22.
- JIANG H, DONG J, ZHANG M, et al. Stress Relaxation Mechanism for Typical Nickel-Based Superalloys Under Service Condition[J]. *Acta Metall Sin*, 2019, 55(9): 1211-1220. (in Chinese)
- FERRERO J G. Candidate materials for high-strength fastener applications in both the aerospace and automotive industries[J]. *Journal of Materials Engineering and Performance*, 2005, 14(6): 691-696.
- SPS TECHNOLOGY. Superalloys Developed by SPS Technologies for Aerospace Fasteners [EB/OL].
- DU J, LV X, DONG J, et al. Research progress of wrought superalloys in China[J]. *Acta Metall Sin*, 2019, 55(9): 1115-1132. (in Chinese)
- SAMIEE M, ASGARI S. Influence of solution treatment on pre-

- precipitation behavior of a Ni-Co alloy[J]. *Scripta Materialia*, 2007, 57(2): 93-96.
- 21 FARVIZI M, ASGARI S. Effects of cold work prior to aging on microstructure of AEREX<sup>TM</sup>350 superalloy[J]. *Materials Science and Engineering: A*, 2008, 480(1): 434-438.
- 22 KERMAJANI M. Influence of double aging on microstructure and yield strength of AEREX<sup>TM</sup> 350[J]. *Materials Science and Engineering: A*, 2012, 534: 547-551.
- 23 LI J, WU Y, LIU Y, et al. Enhancing tensile properties of wrought Ni-based superalloy ATI 718Plus at elevated temperature via morphology control of  $\eta$  phase[J]. *Materials Characterization*, 2020, 169: 110547.
- 24 SHINGLEDECKER J P, PHARR G M. The Role of Eta Phase Formation on the Creep Strength and Ductility of INCONEL Alloy 740 at 1023 K (750 °C)[J]. *Metallurgical and Materials Transactions A*, 2012, 43(6): 1902-1910.
- 25 QI Q, ZHANG H, LIU C, et al. On the microstructure evolution during low cycle fatigue deformation of wrought ATI 718Plus alloy[J]. *Materials Science and Engineering: A*, 2020, 798: 140132.
- 26 HONG H U, KIM I S, CHOI B G, et al. The effect of grain boundary serration on creep resistance in a wrought nickel-based superalloy[J]. *Materials Science and Engineering: A*, 2009, 517(1): 125-131.
- 27 KONTIS P. Influence of composition and precipitation evolution on damage at grain boundaries in a crept polycrystalline Ni-based superalloy[J]. *Acta Materialia*, 2019.
- 28 ASGARI S. Structure and strain hardening of superalloy AEREX350[J]. *Journal of Materials Processing Technology*, 2001, 118(1-3): 246-250.
- 29 ALABBAD B, TIN S. Effect of grain boundary misorientation on  $\eta$  phase precipitation in Ni-base superalloy 718Plus[J]. *Materials Characterization*, 2019, 151: 53-63.
- 30 ZHAO Y, PENG J, ZHANG X, et al. Effect on solution holding time on microstructure and mechanical properties of GH4698 superalloy[J]. *Heat Treatment of Metals*, 2016, 41(8): 56-59. (in Chinese)
- 31 DEVAUX A, NAZÉ L, MOLINS R, et al. Gamma double prime precipitation kinetic in Alloy 718[J]. *Materials Science and Engineering: A*, 2008, 486(1-2): 117-122.
- 32 HOSSEINI E, POPOVICH V A. A review of mechanical properties of additively manufactured Inconel 718[J]. *Additive Manufacturing*, 2019, 30: 100877.
- 33 SLAMA C, ABDELLAOUI M. Structural characterization of the aged Inconel 718[J]. *Journal of Alloys and Compounds*, 2000, 306(1-2): 277-284.
- 34 ZHANG M, MA C C, CHUN X, et al. Effect of Precipitate Phases and Grain Size on Mechanical Properties of Inconel 718 Superalloy After Various Heat Treatments[J]. *Rare Metal Materials and Engineering*, 2024, 53(8): 2131-2136.
- 35 KENNEDY R L. Allvac 718Plus, Superalloy for the Next Forty Years[C]// *Superalloys 718, 625, 706 and Various Derivatives* (2005). TMS, 2005: 1-14.
- 36 HASSAN B, CORNEY J. Grain boundary precipitation in Inconel 718 and ATI 718Plus[J]. *Materials Science and Technology*, 2017, 33(16): 1879-1889.
- 37 KIENL C, MANDAL P, LALVANI H, et al. Role of the Secondary Phase  $\eta$  During High-Temperature Compression of ATI 718Plus®[J]. *Metallurgical and Materials Transactions A*, 2020, 51(8): 4008-4021.
- 38 GÖKEN M, KEMPF M. Microstructural properties of superalloys investigated by nanoindentations in an atomic force microscope[J]. *Acta Materialia*, 1999, 47(3): 1043-1052.
- 39 KINZEL S, GABEL J, VÖLKL R, et al. Reasons for Volume Contraction after Long-Term Annealing of Waspaloy[J]. *Advanced Engineering Materials*, 2015, 17(8): 1106-1112.
- 40 LIU G, XIAO X, VÉRON M, et al. The nucleation and growth of  $\eta$  phase in nickel-based superalloy during long-term thermal exposure[J]. *Acta Materialia*, 2020, 185: 493-506.
- 41 AGNOLI A, LE GALL C, THEBAULT J, et al. Mechanical Properties Evolution of  $\gamma'/\gamma''$  Nickel-Base Superalloys During Long-Term Thermal Over-Aging[J]. *Metallurgical and Materials Transactions A*, 2018, 49(9): 4290-4300.
- 42 WANG M X, ZHU H, YANG G J, et al. Solid-solution strengthening effects in binary Ni-based alloys evaluated by high-throughput calculations[J]. *Materials & Design*, 2021, 198: 109359.
- 43 KOU H, LI W, MA J, et al. Theoretical prediction of the temperature-dependent yield strength of solid solution strengthening Nickel-based alloys[J]. *International Journal of Mechanical Sciences*, 2018, 140: 83-92.
- 44 BUTT M Z. Solid-solution hardening in dilute and concentrated alloys[J]. *Philosophical Magazine Letters*, 1989, 60(4): 141-145.
- 45 GYPEN L A, DERUYTTERE A. The combination of atomic size and elastic modulus misfit interactions in solid solution hardening[J]. *Scripta Metallurgica*, 1981, 15(8): 815-820.
- 46 KRATOCHVÍL P, LUKÁČ P, SPRUŠIL B. On solid solution hardening in crystals with randomly distributed solute atoms[J]. *Czechoslovak Journal of Physics*, 1973, 23(6): 621-626.
- 47 LABUSCH R. A Statistical Theory of Solid Solution Hardening[J]. *physica status solidi (b)*, 1970, 41(2): 659-669.



- 48 FLEISGHER R L. Solution hardening[J]. *Acta metallurgica*, 1961, 9(11): 996-1000.
- 49 FLEISCHER R L. Substitutional solution hardening[J]. *Acta metallurgica*, 1963, 11(3): 203-209.
- 50 MISHIMA Y, OCHIAI S, HAMA O N, et al. Solid Solution Hardening of Ni<sub>3</sub>Al with Ternary Additions[J]. *Transactions of the Japan Institute of Metals*, 1986, 27(9): 648-655.
- 51 ROTH H A, DAVIS C L, THOMSON R C. Modeling solid solution strengthening in nickel alloys[J]. *Metallurgical and Materials Transactions A*, 1997, 28(6): 1329-1335.
- 52 MISHIMA Y, OCHIAI S, HAMA O N, et al. Solid solution hardening of nickel—role of transition metal and B-subgroup solutes—[J]. *Transactions of the Japan institute of metals*, 1986, 27(9): 656-664.
- 53 GYPEN L A, DERUYTTERE A. Multi-component solid solution hardening[J]. *Journal of Materials Science*, 1977, 12(5): 1034-1038.
- 54 CHEN Y T, YEH A C, LI M Y, et al. Effects of processing routes on room temperature tensile strength and elongation for Inconel 718[J]. *Materials & Design*, 2017, 119: 235-243.
- 55 CHEN X M, NING M T, HU H W, et al. Characterization of hot deformation behavior and optimization of hot workability for GH4698 superalloy[J]. *Materials Characterization*, 2023, 201: 112916.
- 56 HOSSEINIFAR M, ASGARI S. Static recrystallization behavior of AEREX350 superalloy[J]. *Materials Science and Engineering: A*, 2010, 527(27): 7313-7317.
- 57 LI K, HAN G, DENG B. Influence of aging treatment on microstructure and properties of cold-drawn alloy GH350[J]. *Acta Aeronautica et Astronautica Sinica*, 2012, 33(06): 1156-1162. (in Chinese)
- 58 YANG C L, ZHANG Z J, ZHANG P, et al. Synchronous improvement of the strength and plasticity of Ni-Co based superalloys[J]. *Materials Science and Engineering: A*, 2018, 736: 100-104.
- 59 GIESE S, BEZOLD A, PRÖBSTLE M, et al. The Importance of Diffusivity and Partitioning Behavior of Solid Solution Strengthening Elements for the High Temperature Creep Strength of Ni-Base Superalloys[J]. *Metallurgical and Materials Transactions A*, 2020, 51(12): 6195-6206.
- 60 FAYMAN Y. C.  $\gamma$ - $\gamma'$  Partitioning Behaviour in Waspaloy[J]. *Materials Science and Engineering*, 1986, 82, 203-215.
- 61 KARUNARATNE M S A, REED R C. Interdiffusion of Niobium and Molybdenum in Nickel between 900 -1300 °C[J]. *Defect and Diffusion Forum*, 2005, 237-240: 420-425.
- 62 JUNG S B, YAMANE T, MINAMINO Y, et al. Interdiffusion and its size effect in nickel solid solutions of Ni-Co, Ni-Cr and Ni-Ti systems[J]. *Journal of Materials Science Letters*, 1992, 11(20): 1333-1337.
- 63 HE C, LIU L, HUANG T, et al. Effect of aging temperature on the secondary  $\gamma'$  precipitation in a model Ni based single crystal superalloy[J]. *Journal of Alloys and Compounds*, 2020, 836: 155486.
- 64 PRÖBSTLE M, NEUMEIER S, FELDNER P, et al. Improved creep strength of nickel-base superalloys by optimized  $\gamma/\gamma'$  partitioning behavior of solid solution strengthening elements[J]. *Materials Science and Engineering: A*, 2016, 676: 411-420.
- 65 KARUNARATNE M S A, CARTER P, REED R C. Interdiffusion in the face-centred cubic phase of the Ni-Re, Ni-Ta and Ni-W systems between 900 and 1300°C[J]. *Materials Science and Engineering: A*, 2000, 281(1-2): 229-233.
- 66 KARUNARATNE M S A, CARTER P, REED R C. On the diffusion of aluminium and titanium in the Ni-rich Ni-Al-Ti system between 900 and 1200°C[J]. *Acta Materialia*, 2001, 49(5): 861-875.
- 67 CHENG Y, ZHAO X, YUE Q, et al. Research Progress of Effects of Mo and W on Ni-based Single Crystal Superalloys[J]. *Rare Metal Materials and Engineering*, 2023, 52(7): 2599-2611.(in Chinese)
- 68 ASGARI S, SHARGHI-MOSHTAGHIN R, SADEGHAHMADI M, et al. On phase transformations in a Ni-based superalloy[J]. *Philosophical Magazine*, 2013, 93(10-12): 1351-1370.
- 69 XIA W, ZHAO X, YUE L, et al. A review of composition evolution in Ni-based single crystal superalloys[J]. *Journal of Materials Science & Technology*, 2020, 44: 76-95.
- 70 LONG H, MAO S, LIU Y, et al. Microstructural and compositional design of Ni-based single crystalline superalloys — A review[J]. *Journal of Alloys and Compounds*, 2018, 743: 203-220.
- 71 ALI M A, LÓPEZ-GALILEA I, GAO S, et al. Effect of  $\gamma'$  precipitate size on hardness and creep properties of Ni-base single crystal superalloys: Experiment and simulation[J]. *Materialia*, 2020, 12: 100692.
- 72 YANG W, YUE Q, CAO K, et al. Negative influence of rafted  $\gamma'$  phases on 750 °C/750 MPa creep in a Ni-based single crystal superalloy with 4% Re addition[J]. *Materials Characterization*, 2018, 137: 127-132.
- 73 SHUI L, JIN T, TIAN S, et al. Influence of precipitate morphology on tensile creep of a single crystal nickel-base superalloy[J]. *Materials Science and Engineering: A*, 2007, 454-455: 461-466.
- 74 WU J, JIANG X, WANG Y, et al. Effects of Ta on microstructural stability and mechanical properties of hot corrosion resistant Ni-based single crystal superalloys during long-term thermal expo-

sure[J]. *Materials Science and Engineering: A*, 2021, 806: 140829.

75 COSTA A M S, OLIVEIRA J P, SALGADO M V, et al. Effect of Ta and Nb additions in arc-melted Co-Ni-based superalloys: Microstructural and mechanical properties[J]. *Materials Science and Engineering: A*, 2018, 730: 66-72.

76 PENG P, LU L, LIU Z, et al. Investigation on the influence of Ta on the microstructure evolution of Ni-based superalloy DZ411 during directional solidification, heat treatment, and long-term aging[J]. *Journal of Alloys and Compounds*, 2022, 920: 165886.

77 XU Y, WANG T, LV X. Effect of Ta and Mo point preference on the  $\gamma'$  phase of Co-Al-W superalloy[J]. *Rare Metal Materials and Engineering*, 2023, 52(11): 3939-3946. (in Chinese)

78 LAI Y, NING L, ZHAO L, et al. Effects of Ta and Co on Microstructural Stability of a Novel High Strength and Hot Corrosion Resistant Single Crystal Superalloys[J]. *Rare Metal Materials and Engineering*, 2024, 53(3): 748-756. (in Chinese)

79 PARK S J, SEO S M, YOO Y S, et al. Effects of Al and Ta on the high temperature oxidation of Ni-based superalloys[J]. *Corrosion Science*, 2015, 90: 305-312.

80 HAN F F, CHANG J X, LI H, et al. Influence of Ta content on hot corrosion behaviour of a directionally solidified nickel base superalloy[J]. *Journal of Alloys and Compounds*, 2015, 619: 102-108.

81 TOMASELLO C M, PETTIT F S, BIRKS N, et al. Precipitation Behavior in AEREX(TM) 350[C]// Superalloys. TMS, 1996:145-51.

82 WAN W, HAN G, DENG B. Influence of solution treatment on microstructure of AEREX350 alloy[J]. *Journal of Iron and Steel Research International*, 2010, 17(3): 67-71.

83 DONG J, LI L, LI H, et al. Effect of extent of homogenization on the hot deformation recrystallization of superalloy ingot in cogging process[J]. *Acta Metall Sin*, 2015, 51(10): 1207-1218. (in Chinese)

84 LIANG X, ZHANG R, YANG Y, et al. An Investigation of the Homogenization and Deformation of Alloy 718 Ingots[C]//Superalloys 718, 625, 706 and Various Derivatives (1994). TMS, 1994: 947-956.

85 ZHANG X, CHEN J, YANG W, et al. Identification of precipitates in the as-cast microstructure and its evolution behavior during homogenization of a difficult-to-deform GH4141 superalloy[J]. *Rare Metal Materials and Engineering*, 2024, 53(1): 136-147. (in Chinese)

86 HAGIHARA K, NAKANO T, UMAKOSHI Y. Plastic deformation behaviour in Ni3Ti single crystals with D024 structure[J]. *Acta Materialia*, 2003, 51(9): 2623-2637.

87 HOU K, OU M, WANG M, et al. Precipitation of  $\eta$  phase and its effects on stress rupture properties of K4750 alloy[J]. *Materials Science and Engineering: A*, 2019, 763: 138137.

88 YANG Z, CHEN Z, LIN Y, et al. Effect of the aging and recrystallization annealing treatment on the forged mixed grain structure of Ni-based superalloy[J]. *Rare Metal Materials and Engineering*, 2023, 52(9): 3147-3152. (in Chinese)

89 WAN W, HAN G, DENG B. Influence of aging treatment on precipitation behavior of  $\eta$  phase in Ni-Co-Cr alloy[J]. *Journal of Iron and Steel Research International*, 2010, 17(1): 64-69.

90 WANG G, SONG W, LIANG J, et al. Effect of heat treatment on microstructure and tensile properties of a new type of Ni-base superalloy designed for additive manufacturing[J]. *Rare Metal Materials and Engineering*, 2024, 53(3): 787-795. (in Chinese)

91 ZHAO J C, RAVIKUMAR V, BELTRAN A M. Phase precipitation and phase stability in Nimonic 263[J]. *Metallurgical and Materials Transactions A*, 2001, 32(6): 1271-1282.

92 KIM I S, CHOI B G, HONG H U, et al. Influence of thermal exposure on the microstructural evolution and mechanical properties of a wrought Ni-base superalloy[J]. *Materials Science and Engineering: A* 2014, 593: 55-63.

93 SMITH T M, ESSER B D, ANTOLIN N, et al. Segregation and  $\eta$  phase formation along stacking faults during creep at intermediate temperatures in a Ni-based superalloy[J]. *Acta Materialia*, 2015, 100: 19-31.

94 SMITH T M, ESSER B D, ANTOLIN N, et al. Phase transformation strengthening of high-temperature superalloys[J]. *Nature Communications*, 2016, 7(1): 13434.

95 TANG L, ZHANG H, GUO Q, et al. The precipitation of  $\eta$  phase during the solution treatments of Allvac 718Plus[J]. *Materials Characterization*, 2021, 176: 111142.

96 SEIFOLLAHI M, RAZAVI S H, KHEIRANDISH Sh, et al. The Mechanism of  $\eta$  Phase Precipitation in A286 Superalloy During Heat Treatment[J]. *Journal of Materials Engineering and Performance*, 2013, 22(10): 3063-3069.

## 镍基变形高温合金 GH4350 的微观结构特征和强化特点综述

金巨烽<sup>1,2</sup>, 赵新宝<sup>1,3</sup>, 赵倩敏<sup>1,2</sup>, 岳全召<sup>1</sup>, 谷月峰<sup>1,3</sup>, 张泽<sup>1,3</sup>

(1. 浙江大学 高温合金研究所 材料科学与工程学院, 浙江 杭州 3110027)

(2. 浙江大学 工程师学院, 浙江 杭州 3110027)

(3. 浙江大学 硅及先进半导体材料全国重点实验室, 浙江 杭州 3110027)

**摘要:** GH4350(AEREX 350)是一种紧固件用镍基变形高温合金, 最高使用温度可达 750°C; GH4350 具备高抗拉强度的同时, 能抗疲劳、抗应力断裂、抗应力松弛和耐腐蚀, 并具备低膨胀系数和缺口敏感性。该合金主要通过固溶强化以及  $\gamma'$  相沉淀强化, 在  $\gamma'$  相析出的同时也会析出少量  $\eta$  相。研究人员指出, 该合金的微观结构对热处理条件包括温度和时间十分敏感,  $\gamma'$  相在某些热处理条件下会转变为  $\eta$  相, 从而可能降低合金的性能。本综述概述了 GH4350 的元素组成特点、受热处理调控的微观结构特征以及强化特点, 旨在理解该合金性能优异的原因, 并指导新型合金或性能优化型合金的开发, 以进一步提高其承温能力。

**关键词:** 紧固件用变形高温合金GH4350; 高温性能; 元素组成; 热处理;  $\eta$ 相

作者简介: 金巨烽, 男, 2000 年生, 硕士, 浙江大学 工程师学院, 浙江 杭州 3110027, 电话: 0571-64219632, E-mail: jinjufeng@zju.edu.cn